PASJ: Publ. Astron. Soc. Japan , 1–**??**,
© 2022. Astronomical Society of Japan.

arXiv:1211.0818v2 [astro-ph.SR] 13 Apr 2013

Discovery of Metastable Helium Absorption Lines in V1280 Scorpii*

Hiroyuki Naito
Graduate School of Science, Nagoya University, Furo-cho, Chikusa-ku, Nagoya 464-8602
naito@stelab.nagoya-u.ac.jp
Akito Tajitsu
Subaru Telescope, National Astronomical Observatory of Japan, 650 North A'ohoku Place, Hilo, HI 96720, USA
Akira Arai
Center for Astronomy, University of Hyogo, Sayo-cho, Sayo, Hyogo 679-5313
and
Kozo Sadakane
Astronomical Institute, Osaka Kyoiku University, Asahigaoka, Kashiwara, Osaka 582-8582

(Received ; accepted)

Abstract

We report the discovery of blue-shifted metastable He I* absorption lines at 3188 Å and 3889 Å with multiple components on high-resolution spectra ($R \sim 60\,000$) of V1280 Scorpii. Similar multiple absorption lines associated with Na I D doublet and Ca II H and K are observed. Na I D doublet absorption lines have been observed since 2009, while the metastable He I* absorption lines were absent in 2009 and were detected in 2011 (four years after the burst). We find different time variations in depths and velocities of blue-shifted absorption components among He I*, Na I, and Ca II. The complex time evolutions of these lines can be explained by assuming changes in density and recombination/ionization rate when the ejecta expand and the photosphere contracts to become hotter. The multiple absorption lines originate in the ejected materials consisting of clumpy components, which obscure a significant part of the continuum emitting region. We estimate the total mass of the ejected material to be on the order of $\sim 10^{-4}$ $M_\odot$, using metastable He I* $\lambda\lambda$3188 and 3889 absorption lines.

Key words: stars: individual: V1280 Sco – novae, cataclysmic variables – mass-loss – winds, outflows

1. Introduction

V1280 Sco (Nova Scorpii 2007 No. 1) is a classical nova which was independently discovered by two Japanese amateur astronomers (Y. Nakamura and Y. Sakurai) on 2007 February 4 at ninth visual magnitude (Yamaoka et al. 2007). Detailed descriptions of photometric and spectroscopic observations from pre-maxium to plateau phase (from February 2007 to April 2011) have been reported in Naito et al. (2012). Recently, Chesneau et al. (2012) reported the presence of a dusty hourglass-shaped bipolar nebula around V1280 Sco based on mid-infrared imaging observations.

A particularly interesting feature of this nova is that it had a exceptionally long plateau spanning over 1500 days, which suggests that V1280 Sco is an extremely slow nova. According to our latest photometric observation in the y band at Osaka Kyoiku University, the nova maintains its brightness ($m_y = 10.45 \pm 0.01$) at least until 2012 August 2 ($\sim$ 66 months after the maximum light). The nova took about 50 months after the burst to enter the nebular phase, which implies that V1280 Sco is the slowest nova in the historical record.

The very long evolutionary time-scale observed in V1280 Sco is in agreement with predictions of slow novae in the optically thick wind model (Kato & Hachisu 1994). The model shows that the decreasing mass loss rate of the nova wind results in an inward moving photosphere and increase in the effective temperature and degree of ionization. In theory, based on the universal decline law propounded by Hachisu & Kato (2006), the speed class of classical novae is mainly determined by the white dwarf (WD) mass; progenitors of slow novae are expected to be lower-mass WDs than fast novae. If the theory is the case, similar burst mechanisms work between slow and fast novae and there could be common (but on a different time scale) features in observational data. It is very important to seek common and/or missing observational features among classical novae to understand the nova phenomenon as a whole. In this respect, V1280 Sco is the best target because it is an extremely slow nova and provides us with a valuable opportunity to investigate its spectral evolution closely.

Sadakane et al. (2010) (hereafter, Paper I) discovered multiple high-velocity narrow Na I D absorption lines on high-resolution spectra obtained in 2009. They suggest that these high-velocity components originated in cool clumpy gas clouds moving on the line-of-sight, produced during interactions between pre-existing cool circumstellar gas and high-velocity gas ejected in the nova explosion. These absorption are useful to investigate the physical

* Based on data collected at the Subaru Telescope, which is operated by the National Astronomical Observatory of Japan.

conditions and time evolution of surrounding circumbinary gas. Similar features of Na I D doublet and Ca II H and K lines are observed in many other classical novae during the early phase (Williams et al. 2008), while the survival time (several years) of Na I D absorption lines in V1280 Sco is much longer than those observed among fast novae (within several weeks or months). To investigate the difference on multiple absorption lines between V1280 Sco (slow nova) and fast novae, we have continued high-resolution spectroscopic observations for four years (2009 – 2012).

In this paper, we report the discovery of blue-shifted metastable He I* absorption lines and investigate time variations of He I*, Na I D and Ca II lines from 2009 to 2012. Our spectral observations are summarized in section 2. We focus on the discovery of multiple metastable He I* absorption lines in section 3, and co-existance of He I*, Na I and Ca II lines are described in section 4. We discuss the origins of discrete absorption lines and the structure of ejected shell in section 5, and conclusions are given in section 6.

2. Observations and data reduction

High-resolution spectroscopic observations of V1280 Sco were performed using the 8.2-m Subaru telescope equipped with the High Dispersion Spectrograph (HDS; see Noguchi et al. 2002 for details) from 2009 to 2012. This period corresponds to the long plateau phase shown in Fig. 1, which includes photometric data obtained in 2012 at Osaka Kyoiku University. Table 1 provides a journal of the observations, in which the observing dates are listed in the universal time at the start time of the exposure. We have obtained 21 spectra under 5 configurations of the spectrograph, which cover the wavelength region from 3030 Å to 8070 Å and provide the typical resolving power of $R \cong 60\,000$ at Hα. The slit width is 0".6 (0.3 mm). Data reduction was carried out using the IRAF[1] software package in a standard manner. The wavelength calibration was performed using the Th-Ar comparison spectrum obtained during each observation. Spectrophotometric calibration was performed using the spectrum of HIP 83740 (A0 III) obtained at nearly same altitude of V1280 Sco on the same nights, with exceptions of the data obtained in 2009 May and 2011 March due to hazy weather conditions. All spectra were converted to the helio-centric scale. Corrections for interstellar extinction have not been applied.

3. Confirmation of metastable He I* absorption lines

We reported in Paper I the discovery of multiple high-velocity circumstellar absorption lines of Na I D2 and D1 on high-resolution spectra observed in 2009. We analyzed additional spectra ranging from 3030 Å to 8070 Å to look for similar absorption features associated with other elements. We found such blue-shifted multiple absorption lines corresponding to metastable He I* $\lambda\lambda$3188, 3889 and Ca II H and K. Multiple absorption lines of Na I and Ca II have been discussed in the literatures (e.g. Williams et al. 2008; Williams & Mason 2010), those of the metastable He I* have never been reported in classical novae.

Figure 2 shows the spectral region between 3820 Å and

[1] IRAF is distributed by NOAO for Research in Astronomy, Inc., under cooperative agreement with the National Science Foundation.

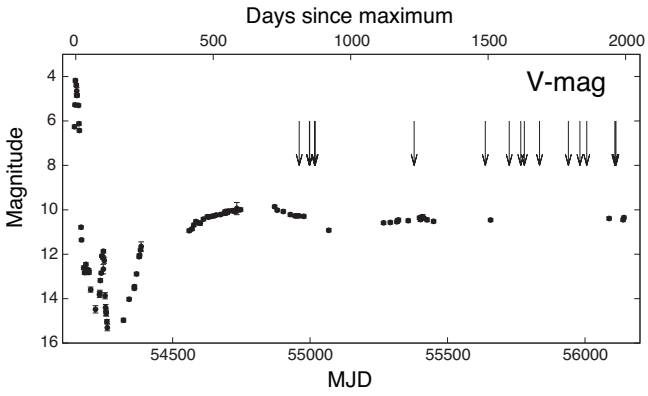


Fig. 1. Light curve of V1280 Sco observed at Osaka Kyoiku University. The epochs of our spectroscopic observations are indicated by arrows.

Table 1. Journal of spectroscopic observations of V1280 Sco.

Date	UT h m	MJD	Exposure sec	Range Å
2009				
May 9	12 24	54 960.517	900	4100-6860
Jun. 15	12 36	54 997.525	600	4100-6860
Jun. 16	6 45	54 998.282	900	3400-5110
	11 48	54 998.492	900	4110-6870
	12 14	54 998.510	900	5310-8070
Jul. 4	10 51	55 016.452	900	4100-6860
Jul. 6	9 19	55 018.389	1200	4100-6860
	10 37	55 018.443	600	3400-5110
2010				
Jul. 1	9 43	55 378.405	1200	4130-6860
2011				
Mar. 17	15 27	55 637.644	930	4100-6860
Jun. 12	10 33	55 724.440	1200	4100-6860
Jul. 24	6 36	55 766.275	1800	4100-6860
Aug. 6	5 43	55 779.239	1200	4100-6860
	6 39	55 779.277	1200	3030-4630
Sep. 30	5 39	55 834.236	2400	4130-6860
2012				
Jan. 13	16 17	55 939.679	137	5080-7850
Feb. 24	15 29	55 981.645	1800	4100-6860
Mar. 20	14 41	56 006.612	1200	4100-6860
	15 14	56 006.635	1800	3400-5110
Jun. 30	7 53	56 108.328	1200	3540-5250
Jul. 4	10 3	56 112.419	600	4100-6860

UT: Universal time at the start time of an exposure

3900 Å obtained on 2009 June 16, 2011 August 6, and 2012 March 20. These spectra show a continuum with H I, Fe II, and Si II lines in emission. While there are neither appearances nor disappearances of major emission lines, multiple absorption lines around 3880 Å (shifted by ~ -700 km s^{-1} from 3889 Å) are detected in 2011 and 2012. The feature is not observed in 2009. To examine whether blue-shifted components of H I λ3889 (H8) can be responsible for these absorption lines, we examine the presence of absorption features expected at the corresponding wavelengths for H I λ3835 (H9). There is no signature of absorption for the H9 line. Therefore, we guess the multiple absorption lines as those of the metastable He I* λ3889.

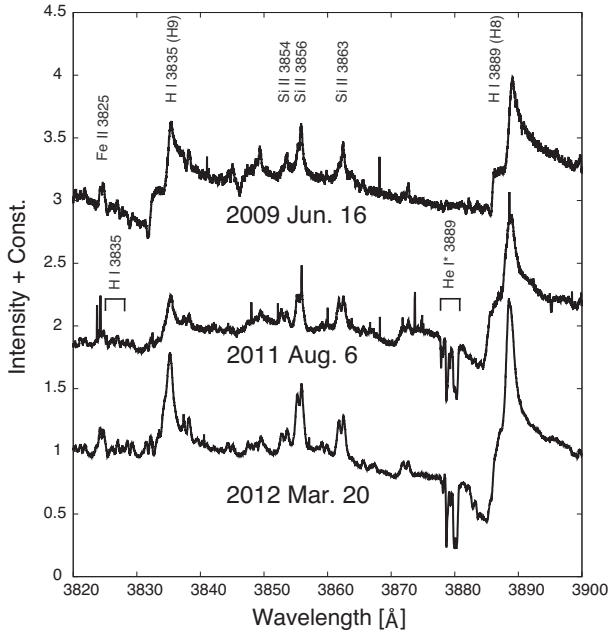


Fig. 2. Detection of multiple absorption lines around He I* λ3889 in 2011 and 2012. These absorption lines originate from the metastable He I*. Blue-shifted absorptions of the H I line at 3889 Å (H8) are negated because no corresponding absorptions can be found at H9.

Since both He I* $\lambda\lambda$3188 and 3889 arise from the same metastable state 2 ^{3}S, a similar set of absorption features is expected to be seen in He I* λ3188. Figure 3 shows a comparison of multiple high-velocity absorption lines in the He I* $\lambda\lambda$3188 and 3889 observed on 2011 August 6. While the signal-to-noise ratio for He I* λ3188 is rather low, we can see exact coincidences of four major absorption features (components A, B, L, and N). Thus, the identification of He I metastable lines in V1280 Sco can be definitely concluded.

As far as we know, the He I* λ3889 absorption line has been reported only in the the recurrent nova U Sco (Johnston & Kulkarni 1992). However, the observed velocity in U Sco (~ -120 km s^{-1}) is significantly lower than those of V1280 Sco. Johnston & Kulkarni (1992) suggested that the He I* absorption dose not originate in the ejected shells but from a corona around the secondary star in U Sco system. Hence, we conclude that our observation is the first detection of metastable He I* absorption lines originating in the ejected (circumstellar) gas around novae.

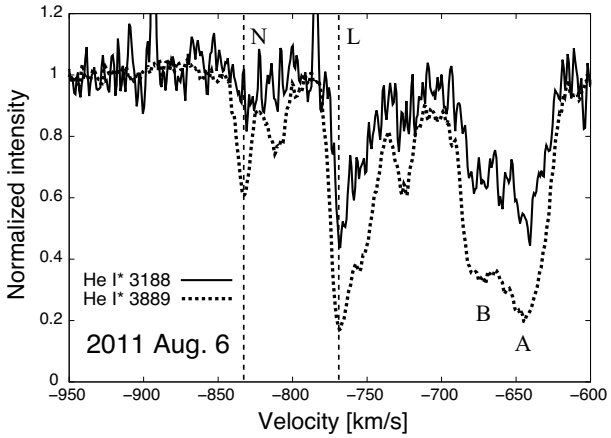


Fig. 3. Comparison of multiple blue-shifted high-velocity absorption components originating from metastable He I* λ3188 and He I* λ3889 observed on 2011 August 6. Both lines arise from the same triplet metastable level (2 ^{3}S) of He I. Although the signal-to-noise level for He I* λ3188 is much lower, there is little doubt that both lines show the same absorbing components.

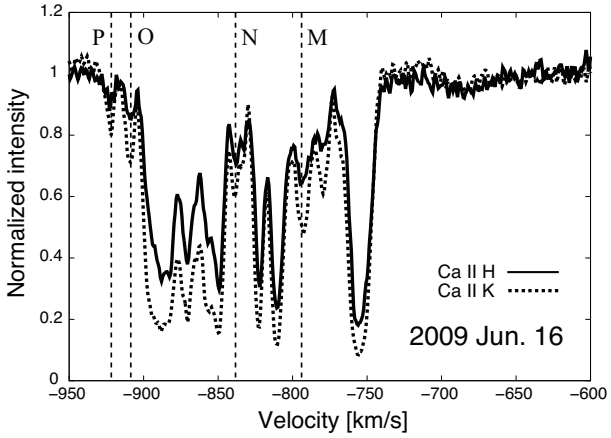


Fig. 4. Comparison of multiple blue-shifted high--velocity absorption components originating from Ca II H and K observed on 2009 June 16.

4. Co-existence of He I*, Na I, and Ca II absorption lines

We have discovered at least eleven discrete high-velocity absorption components in the Na I D doublet on the high-resolution spectra observed in 2009 (in Paper I). We find

that similar high-velocity absorption lines can be seen in Ca II H and K on the high-resolution spectra observed in 2009 (Fig. 4). It is interesting to find at least four new absorption features in Ca II H and K lines which have not been noticed in Paper I. They are components M, N, O, and P in Fig. 4. The component P is displaced by −922 km s^{-1}, which is higher by ∼ 40 km s^{-1} than the fastest component found in the Na I D absorptions.

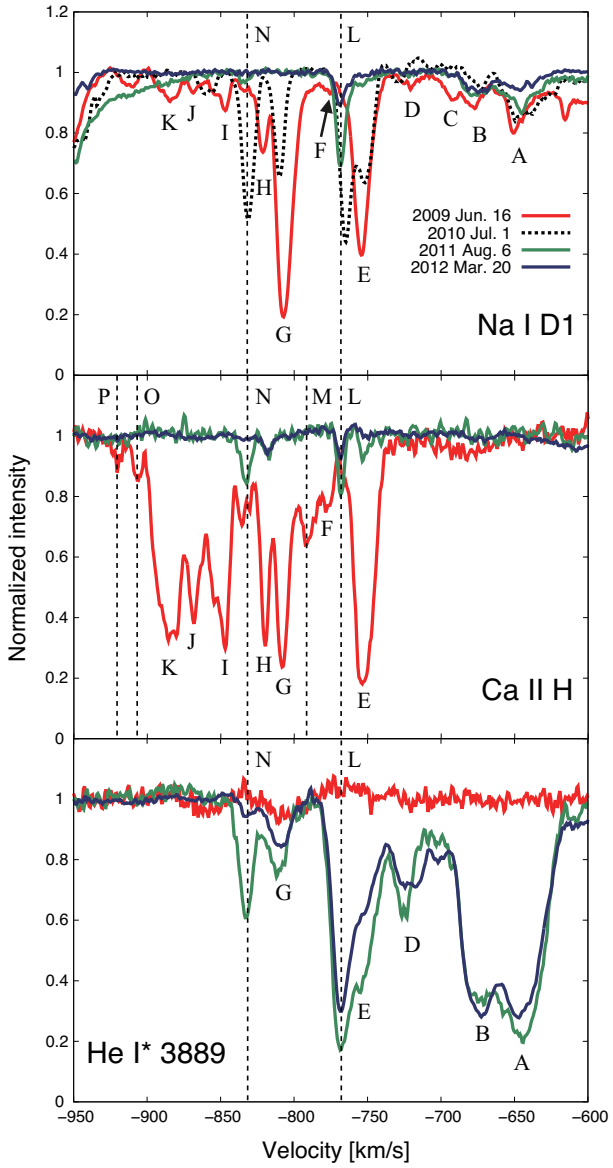


Fig. 5. Developments of absorption profiles of Na I D1, Ca II H, and He I* λ3889 from 2009 to 2012. Components A, B, C, D, E, F, G, H, I, J, and K are introduced which are associated with those in Paper I. Components L, M, N, O, and P are the same as Figs. 3 and 4. We have no data for Ca II H and He I* λ3889 in 2010.

Figure 5 shows comparison of absorption profiles of Na I D1, Ca II H, and He I* λ3889 observed from 2009 through 2012. Components A through K are the same as noted in Paper I. For He I* lines, four major absorption components are identified in the 2011 spectra (noted as A, B, L, and N in Fig. 3). Two new absorption components L and N of Na I D developed in 2010. Temporal variations in both wavelengths and strengths among these spectra illustrate complex changes in column density and velocity for each component. Measurements of the velocities and the depths of discrete absorption components are tabulated in Table 2. Errors in measurements are estimated to be ± 5 km s^{-1} in velocity and ± 0.02 in depth.

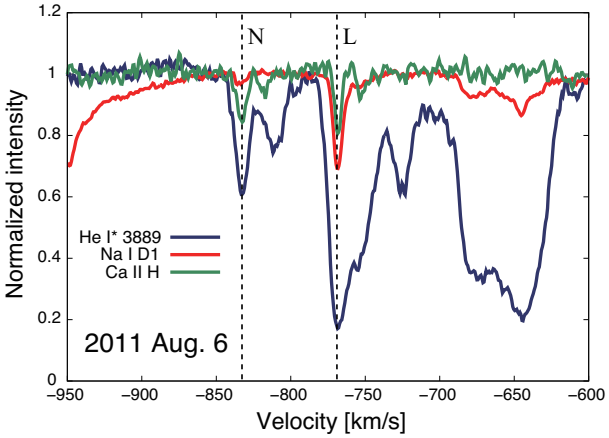


Fig. 6. Profiles of blue-shifted high-velocity absorption components of He I* λ3889, Na I D1, and Ca II H on 2011 August 6. Each absorption component is noted as in Fig. 3. Components L and N are seen in all the species on 2011 August 6.

On the component G of Na I D1, we find that the depth becomes shallower (from 0.81 to 0.34), and the line center is shifted (from 806.1 km s^{-1} to 809.2 km s^{-1}) from 2009 to 2010. Similar changes are noted in the components A, B, E, and L. These findings might indicate that the broader components consist of several narrow lines coming from smaller clumpy clouds having different velocities, and the observed variation in velocity can be interpreted as due to change of contributing ratio of each clumpy component. There seems no acceleration mechanism for the particular components during the early period as suggested by Williams (2011). The fact that the deepest absorption lines for all elements show a certain level of intensity (∼ 0.2) at line centers indicates that the covering factor of combined components is at least larger than 0.8 (see Sect. 5.2).

Metastable He I* absorption lines are observed in other astronomical objects such as Seyfert galaxies (e.g. Markarian 231: Boksenberg et al. 1977; NGC 4151: Anderson & Kraft 1969; Anderson 1974), quasars (e.g. QSO 2359−1241: Arav et al. 2001), or nebula (e.g. the Orion Nebula: Wilson et al. 1959). Anderson (1974) gives a conclusion that He I* absorption features arise in the region characterized by higher electron density ($> 10^6$ cm^{-3}) in NGC 4151. The Seyfert galaxy Markarian 231 shows multiple absorption lines of He I* λ3889, Na I D and Ca II H and K (Boksenberg et al. 1977) and similar features – co-existence of He I*, Na I, and Ca II originating in

absorbing shells – are observed in components L and N of V1280 Sco (Fig. 6). Figure 6 shows that He I* absorptions are much stronger than either Na I or Ca II absorptions in all of the absorption systems, which demonstrates that the most parts of the absorbing clouds are strongly ionized by a high-temperature radiation source.

5. Discussion

Recent high-resolution spectroscopic observations have revealed that narrow, time-variable Na I D absorption features are exhibited in some kinds of cataclysmic variable systems, i.e., novae (e.g. V1280 Sco: Paper I; RS Oph: Patat et al. 2011; T Pyx: Shore et al. 2011; V407 Cyg: Shore et al. 2012) and type Ia supernovae (e.g. SN 2006X: Patat et al. 2007; SN 1999cl: Blondin et al. 2009; SN 2007le: Simon et al. 2009; PTF 11kx: Dilday et al. 2012). The origins of the absorption lines are presently controversial, however, these lines could be used to investigate the structure and evolution of circumstellar environment around progenitor systems with the implication for physical connections among various types of cataclysmic variables.

According to Williams & Mason (2010), multiple high-velocity absorption lines of Na I D doublet are observed in ~ 80 % of classical novae. These lines weaken and disappear within several weeks/months after the maximum light. Most of the novae with such absorption lines exhibit a gradual outward acceleration in the weeks following the maximum light. While being common among novae, the physical nature of these lines have been scarcely discussed. Two scenarios for the origins of these absorption lines are proposed in Williams (2011): (1) a pre-existing circumbinary reservoir before the nova outburst, or (2) outflowing high-density blobs associated with post-outburst ejecta. Since multiple absorption systems are expected to appear and disappear in different ways, more time-sequence observational data of many novae could discriminate between the two scenarios (Williams 2011). Another interpretation accounting for the observed behavior of absorption lines is presented by Shore et al. (2011). They argue that the time sequence of absorption lines can be explained in a situation where recombination and/or ionization fronts move outward in the expanding gas. The scenario is based on the study of recurrent nova T Pyx, which exhibits massive ejecta in each event.

In this section, we discuss the origins of discrete absorption lines and structure of ejected shell of V1280 Sco using metastable He I* absorption lines along with Na I D doublet and Ca II H and K. This new approach can be widely employed to probe the circumstellar structure of cataclysmic variables.

5.1. Survival time of discrete absorption lines

Some components corresponding to Na I D1 and Ca II H (components A and B) weakened significantly from 2009 to 2012. On the other hand, these two components of He I* λ3889 were absent in 2009 and remarkably grown in 2011 and 2012. Survival time of these absorption lines in V1280 Sco is an order of years, which is much longer than those observed among fast novae (an order of weeks or months). Furthermore, He I* λ3889 absorption lines were detected for the first time in 2011, four years after the maximum light. These behavior associated with He I* can be understood that the number of ultraviolet photons had increased significantly to produce singly-ionized helium as the central photosphere shrinks to become hotter. Consequently, we postulate that the complex evolutions of multiple absorption lines are due to combined changes in physical conditions, such as the density, recombination and ionization rate, for each component. Considering that V1280 Sco had taken a very long time to emit ultraviolet radiation extensively (Naito et al. 2012), the most significant parameter extending the survival time of multi absorption lines of Na I D and Ca II H and K – low excitation lines– could be the ionization rate caused by a change in the temperature of the photosphere.

5.2. Column density of He (2 ^3S)

Metastable He I* lines are often used to derive physical parameters of nebulosity because processes of transition are well understood. Of the recombinations to excited levels of He I, approximately three-quarters are led to the triplet levels and approximately one-quarters are led to the singlet levels. All electrons in the triplets are led ultimately to 2 ^{3}S through downward radiative transitions, which is highly metastable (Osterbrock & Ferland 2006). Since both He I* λ3188 and He I* λ3889 are transitions from the same metastable level, the ratio of optical depths is fixed by atomic physics, provided that the lines are not saturated. If we adopt the partial covering model used in Leighly et al. (2011), the following relations are obtained:

$$R_{3188} = (1 - C_{\rm f}) + C_{\rm f} e^{-\tau_{3188}} \quad (1)$$

$$R_{3889} = (1 - C_{\rm f}) + C_{\rm f} e^{-\tau_{3889}} \quad (2)$$

where R is the ratio of the observed spectrum intensity to the continuum, $C_{\rm f}$ is the fraction of the continuum source which is covered by the absorbing clumpy gas (the covering factor), and τ_{3188} and τ_{3889} are the optical depths of He I* λ3188 and He I* λ3889, respectively. All of these parameters are functions of velocity. When we know the optical depth τ at line center, the column density N can be derived from the following expression given in Rudy et al. (1985):

$$N = (\tau b)/(0.015 \lambda f_{12}) \quad (3)$$

where λ is the wavelength in cm, f_{12} is the oscillator strength, and b is a measure of the velocity width in units of cm s^{-1}. The column density of the 2 ^{3}S level can be transformed into the column density of He^+ using the relation given in Clegg (1987):

$$\frac{N(2\ ^3{\rm S})}{N({\rm He}^+)} = \frac{5.79 \times 10^{-6} t_{\rm e}^{-1.18}}{1 + 3110 t_{\rm e}^{-0.51} n_{\rm e}^{-1}} \quad (4)$$

where $t_{\rm e}$ is the electron temperature in 10^4 K and $n_{\rm e}$ is the electron density in cm^{-3}. When we use a typical value of 10^4 K for the electron temperature, the ratio of $N(2\ ^3{\rm S})$

Table 2. Velocities and depths of absorption components.

Component†		Velocity (km s^{-1})				Depth			
		2009	2010	2011	2012	2009	2010	2011	2012
A	Na I D1	−650.0	−649.0	−644.9	−646.9	0.20	0.16	0.13	0.06
	Ca II H	...		...	...	...		...	...
	He I* 3889	...		−644.4	−647.2	...		0.80	0.72
B	Na I D1	−678.5	−671.9	−676.0	−673.3	0.12	0.06	0.07	0.06
	Ca II H	...		...	...	...		...	...
	He I* 3889	...		−672.2	−672.4	...		0.67	0.72
C	Na I D1	−691.3	...	...	...	0.09	...	...	...
	Ca II H	...		...	...	...		...	...
	He I* 3889	...		...	...	...		...	...
D	Na I D1	−720.2	...	...	...	0.06	...	...	...
	Ca II H	...		...	...	...		...	...
	He I* 3889	...		−724.6	−720.8	...		0.39	0.29
E	Na I D1	−753.8	−751.7	...	...	0.61	0.37	...	...
	Ca II H	−753.7		−753.1	...	0.82		0.08	...
	He I* 3889	...		−754.7	...	...		0.64	...
F	Na I D1	−776.7	...	...	...	0.07	...	...	...
	Ca II H	−779.6		...	...	0.24		...	...
	He I* 3889	...		...	...	...		...	...
G	Na I D1	−806.1	−809.2	...	...	0.81	0.34	...	...
	Ca II H	−807.5		...	...	0.76		...	...
	He I* 3889	...		−810.2	−808.3	...		0.25	0.16
H	Na I D1	−820.9	...	...	...	0.27	...	...	...
	Ca II H	−818.8		−817.5	−817.3	0.69		0.06	0.06
	He I* 3889	...		...	...	...		...	...
I	Na I D1	−846.3	...	...	...	0.13	...	...	...
	Ca II H	−846.8		...	...	0.70		...	...
	He I* 3889	...		...	...	...		...	...
J	Na I D1	−868.2	...	...	...	0.07	...	...	...
	Ca II H	−867.9		...	...	0.62		...	...
	He I* 3889	...		...	...	...		...	...
K	Na I D1	−882.9	...	...	...	0.09	...	...	...
	Ca II H	−883.2		...	...	0.67		...	...
	He I* 3889	...		...	...	...		...	...
L	Na I D1	...	−763.9	−767.5	−768.5	...	0.56	0.30	0.11
	Ca II H	...		−767.4	−768.2	...		0.19	0.07
	He I* 3889	...		−767.0	−767.5	...		0.83	0.70
M	Na I D1	...	...	...	...	...	...	...	...
	Ca II H	−790.9		...	...	0.35		...	...
	He I* 3889	...		...	...	...		...	...
N	Na I D1	−833.6	−830.5	−833.1	...	0.06	0.46	0.03	...
	Ca II H	−833.7		−832.4	...	0.27		0.16	...
	He I* 3889	...		−832.5	−832.7	...		0.39	0.06
O	Na I D1	...	...	...	...	...	...	...	...
	Ca II H	−905.8		...	...	0.13		...	...
	He I* 3889	...		...	...	...		...	...
P	Na I D1	...	...	...	...	...	...	...	...
	Ca II H	−922.4		...	...	0.11		...	...
	He I* 3889	...		...	...	...		...	...

†: Components A, B, C, D, E, F, G, H, I, J, and K are labeled as in Paper I.

Table 3. Measured parameters for components of A, B, and L using both metastable He I* λλ3188 and 3889 lines.

Component	Velocity (km s^{-1})	C_f	τ_{3188}	τ_{3889}	b (10^6 cm s^{-1})	$N(2\ ^3S)$ (10^{13} cm^{-2})	$N(He^+)$ (10^{19} cm^{-2})	
							$n_e = 10^5$	$n_e = 10^6$
A	−644.4	0.93	0.98	2.94	1.2 ± 0.5	9.3 ± 3.9	1.7	1.6
B	−672.2	0.95	0.63	1.90	1.6 ± 0.5	7.8 ± 2.4	1.4	1.3
L	−767.0	0.86	1.19	3.56	1.0 ± 0.6	9.8 ± 5.9	1.7	1.7

to $N(He^+)$ can be confined $\sim 10^{-6}$ for the low electron density ($n_e \sim 10^5 - 10^6$; see Appendix 1 for details). Measured parameters for components of A, B, and L are listed in Table 3, where we calculate for two cases of $n_e = 1 \times 10^5$ and $n_e = 1 \times 10^6$, respectively. We find that the column density of He^+ of each component is $\sim 10^{19}$ cm^{-2} for both electron densities.

5.3. Structure and mass of ejected shell

Chesneau et al. (2012) obtained high-spatial resolution mid-infrared images with the Very Large Telescope from 2009 to 2011, showing the dusty nebular around V1280 Sco is bipolar. They suggested that the intensities of two bipolar lobes are different due to an absorption effect; the southern lobe is closer to the observer than the northern one. It is implied that a large part of ejected mass is included in these bipolar lobes. Combined with the presence of absorbing gases on the line-of-sight shown in our observations, we can describe the structure of ejected shell as Fig. 7. We aim to estimate the mass of ejected shell assuming that the components showing He I* λλ3188 and 3889 originate from clumpy gas ejected at the time of the explosion in 2007. As noted in Sect. 5.2, each absorption component covers most of the continuum radiating region (photosphere and free-free emission region) on the line-of-sight and extended $\sim 1 \times 10^9$ km (~ 10 AU) in the past ∼1600 days with the velocity dispersion (FWHM) of $\Delta 10$ km s^{-1}. To achieve the column density of He^+ of $\sim 10^{19}$ cm^{-2}, the following physical condition is needed for the absorbing clumpy gas; (i) $n_e \sim 10^6$ for the solar abundance of He or (ii) $n_e \sim 10^5$ for helium-rich composition. If condition (ii) is the case, the clumpy gas could consist of helium-rich component ejected after hydrogen burning, which is consistent with normal nova phenomena. Supposing the density in individual clumpy gas is uniform, we can estimate the total mass of ejected shell to be on the order of $10^{-4} M_\odot$ by integrating absorption components ranging from −650 km s^{-1} to −920 km s^{-1}. This is derived by a distance-independent method and is consistent with the results of Chesneau et al. (2008) and Naito et al. (2012).

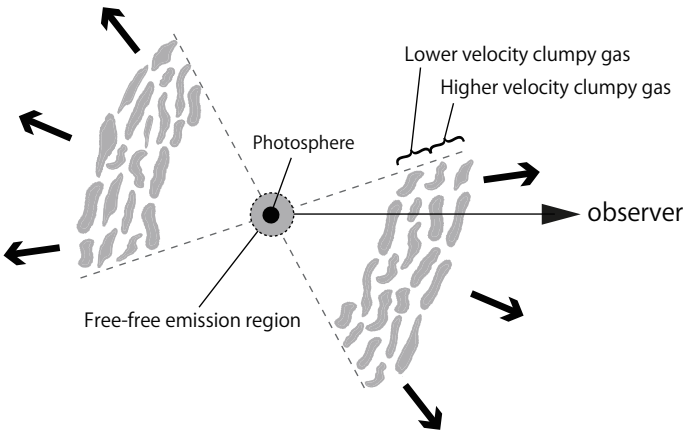


Fig. 7. Schematic of ejected shell (clumpy gas) producing absorption lines of metastable He I* λλ3188 and 3889. Components A and B originate in lower velocity clumpy gases and components L and N originate in higher velocity clumpy gases. Thin broken lines delineate boundaries of the nebula (Chesneau et al. 2012).

6. Conclusions

We performed high-resolution spectroscopic observations of V1280 Sco from 2009 to 2012 and discovered multiple absorption lines corresponding to metastable He I* λλ3188 and 3889. These lines have corresponding absorption components in blue-shifted Na I D doublet and Ca II H and K on the spectra of V1280 Sco. Multiple absorption lines originate in ejected shells consisting of clumpy components which cover a large part of the continuum radiating region (photosphere and free-free emission region) on the line-of-sight. The complex evolution of multiple absorption lines can be explained by the result of changing in density and recombination/ionization rate when the shell expands and the photosphere shrinks to become hotter. We estimate the total mass of ejected shell to be on the order of $\sim 10^{-4}$ $M_\odot$ using metastable He I* λλ3188 and 3889 absorption lines.

We are grateful to students at Osaka Kyoiku University for performing the photometric observations in 2011 and 2012. We sincerely thank Takashi Iijima and Hitoshi Yamaoka for useful comments. Thanks are also due to Kazunori Ishibashi and Shinjirou Kouzuma for careful reading of the manuscript and suggestions. This work was supported by the Global COE Program of Nagoya University "Quest for Fundamental Principles in the Universe (QFPU)" from JSPS and MEXT of Japan.

Appendix 1. Estimation of the electron density in absorption components

According to Williams (2011), velocities of multiple absorption lines almost always correspond to half the veloc-

ities measured from forbidden emission line widths. This fact supports an assumption that these absorption and forbidden lines arise from the same region. Intensity ratios of forbidden lines for [O II] and [O III] are expressed as functions of the electron density (n_e) and electron temperature (t_e) as below. Peimbert (1967) gives the expression for [O II];

$$\frac{I(\lambda7320+\lambda7330)}{I(\lambda3726+\lambda3729)} = \frac{\epsilon}{13.70}\frac{1+23.8x(1+0.23\epsilon)+61.2x^2(1+0.61\epsilon+0.07\epsilon^2)}{1+0.13\epsilon+5.3x(1+0.60\epsilon+0.07\epsilon^2)}, \quad \text{(A1)}$$

where

$$x = 10^{-2} n_e {t_e}^{-1/2}, \quad \text{(A2)}$$

and

$$\epsilon = \exp(-19600/t_e). \quad \text{(A3)}$$

Osterbrock & Ferland (2006) give the expression for [O III];

$$\frac{I(\lambda4363)}{I(\lambda4959+\lambda5007)} = \frac{1+4.5\times10^{-4} n_e/{t_e}^{1/2}}{7.90\exp(3.29\times10^4/t_e)}. \quad \text{(A4)}$$

When the intensity ratios of [O II] and [O III] are measured, the electron density and the electron temperature in absorption components can be derived.

Hence [O II] 3726, 3729 and [O III] 4363 lines are not detected in our spectra, the intensity ratios are not able to be measured exactly. However, we can set a limitation on the physical parameters by considering the detection limits for such weak forbidden lines. When an interstellar correction of $B(E-V) = 0.4$ is applied (Naito et al. 2012), the condition of both $I(\lambda7320+\lambda7330)/I(\lambda3726+\lambda3729) > 0.86$ and $I(\lambda4363)/I(\lambda4959+\lambda5007) < 0.015$ is set to be satisfied. Adopting $\sim 10^4$ K as a typical value for the electron temperature, the electron density can be confined somewhere between 10^5 and 10^6 cm^{-3} (see Fig. 8).

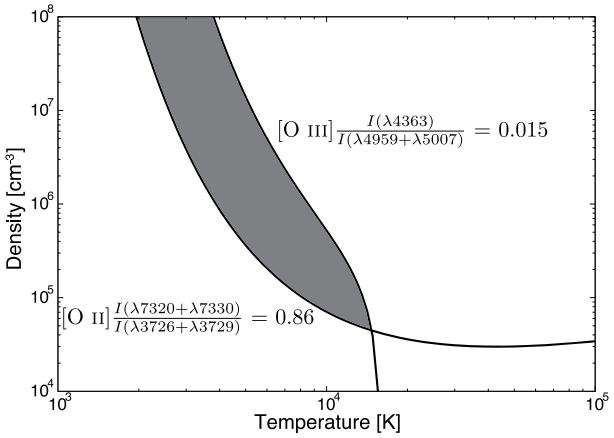


Fig. 8. Permitted area for the electron temperature and the electron density. The colored zone between two lines satisfies the conditions from [O II] and [O III] forbidden lines.

References

Anderson, K. S. 1969, ApJ, 158, 859

Anderson, K. S. 1974, ApJ, 189, 195

Arav, N., Brotherton, M. S., Becker, R. H., Gregg, M. D., White, R. L., Price, T., & Hack, W. 2001, ApJ, 546, 140

Blondin, S., Prieto, J. L., Patat, F., Challis, P., Hicken, M., Kirshner, R. P., Matheson, T., & Modjaz, M. 2009, ApJ, 693, 207

Boksenberg, A., Carswell, R. F., Allen, D. A., Fosbury, R. A. E., Penston, M. V., & Sargent, W. L. W. 1977, MNRAS, 178, 451

Chesneau, O., et al. 2008, A&A, 487, 223

Chesneau, O., et al. 2012, A&A, 545, A63

Clegg, R. E. S. 1987, MNRAS, 229, 31p

Dilday, B., et al. 2012, Science, 337, 942

Hachisu, I., & Kato, M. 2006, ApJS, 167, 59

Johnston, H. M., & Kulkarni, S. R. 1992, ApJ, 396, 267

Kato, M., & Hachisu, I. 1994, ApJ, 437, 802

Leighly, K. M., Dietrich, M., & Barber, S. 2011, ApJ, 728, 94

Naito, H., et al. 2012, A&A, 543, A86

Noguchi, K., et al. 2002, PASJ, 54, 855

Osterbrock, D. E., & Ferland, G. J. 2006, in Astrophysics of gaseous nebulae and active galactic nuclei, 2nd., ed. D.E. Osterbrock & G.J. Ferland (Sausalito, California: University Science Books)

Patat, F., et al. 2007, Science, 317, 924

Patat, F., Chugai, N. N., Podsiadlowski, P., Mason, E., Melo, C., Pasquini, L. 2011, A&A, 530, A63

Peimbert, M. 1967, ApJ, 150, 825

Rudy, R. J., Stocke, J. T., & Foltz, C. B. 1985, ApJ, 288, 531

Sadakane, K., Tajitsu, A., Mizoguchi, S., Arai, A., & Naito, H. 2010, PASJ, 62, L5 (Paper I)

Shore, S. N., Augusteijn, T., Ederoclite, A., & Uthas, H. 2011, A&A, 533, L8

Shore, S. N., Wahlgren, G. M., Augusteijn, T., Liimets, T., Koubsky, P., Šlechta, M., & Votruba, V. 2012, A&A, 540, A55

Simon, J. D, et al. 2009, ApJ, 702, 1157

Williams, R., Mason, E., Della Valle, M., & Ederoclite, A. 2008, ApJ, 685, 451

Williams, R., & Mason, E. 2010, Ap&SS, 327, 207

Williams, R. 2011, astro-ph:arXiv1108.4917

Wilson, O. C., Minich, G., Flather, E., & Coffeen, M. F. 1959, ApJS, 4, 199

Yamaoka, H., Nakamura, Y., Nakano, S., Sakurai, Y., & Kadota, K. 2007, IAU Circ., 8803, 1